Hindawi
Geofluids
Volume 2023, Article ID 5039604, 22 pages
https://doi.org/10.1155/2023/5039604

Research Article

The Exquisite Comparison of Shale Mineralogical-Geochemical Characteristics between Chang 7 Member and Chang 9 Member in Yanchang Formation, Ordos Basin

Wang Zhang,[1] **Xinping Liang**,[2] **Peng Li**,[3] **and Guoheng Liu**[4]

[1]*Key Laboratory of Petroleum Resources Research, Institute of Geology and Geophysics, Chinese Academy of Sciences, China*
[2]*Institute of Energy, Peking University, Beijing 100871, China*
[3]*State Key Laboratory of Shale Oil and Gas Enrichment Mechanisms and Effective Development, SINOPEC, Beijing 100083, China*
[4]*School of Geosciences, China University of Petroleum (East China), Qingdao 266580, China*

Correspondence should be addressed to Wang Zhang; zhangwang@mail.iggcas.ac.cn

Received 10 October 2022; Revised 27 March 2023; Accepted 25 July 2023; Published 16 August 2023

Academic Editor: Jin Qian

Significant amounts of unconventional oil and gas resources have been discovered in the Yanchang Formation of Ordos Basin. Shale layers deposited in Chang 7 member (divided into Chang 7-2 submember (C7-2SM) and Chang 7-3 submember (C7-3SM) and Chang 9 member (C9M)) are the main source rocks. Based on the comparison of mineralogical and geochemical characteristics, it is concluded that (1) in terms of mineralogical characteristics, the C7-3SM shale possesses the largest content of illite/smectite mixed layer and reducing minerals and the least quantity of quartz. The C9M shale shows the highest percentage of quartz and illite and the least amount of K-feldspar and Kaolinite. In C7-2SM and C9M shale, amorphous silica surrounded tightly by clay minerals is easily observed by the scanning electron microscopy. Besides the drilling orientation, the small content of quartz contributed to the lowest porosity for the C7-3SM shale. (2) In terms of geochemical characteristics, the C7-3SM shale exhibits high productivity due to type II_1 kerogen. The organic matter in the C7-2SM and C9M shale contains mainly type II_2 and possibly type III kerogen. The C9M shale exhibits the highest organic thermal maturity. The C7-3SM shale was formed in a relatively higher salinity of sedimentary water.

1. Introduction

Successful exploration of shale gas in previous years has aroused wide public concern about the shale reservoir [1–4]. In recent years, the lacustrine shale gas exploration also succeeded in the Permian Lucaogou Formation of Junggar Basin, the Mesozoic Yanchang Formation of Ordos Basin and the Upper Cretaceous Qingshankou Formation of Songliao Basin. Along with these exploration practices, a lot of research findings have been produced [5–8]. The lacustrine shale is different from marine shale in many aspects, including the structural and depositional setting, pore and fracture networks, geochemical and reservoir characteristics, shale gas genetic types, and accumulation model [9–12].

Globally, only 1.2% of Phanerozoic source rocks are Triassic in origin. However, the Triassic Yanchang Formation of the Ordos Basin having the large abundant shale oil resources in China [13, 14]. Shale layers, the most important source rock in the Ordos Basin, are primarily deposited in Chang 9 and Chang 7 members. In recent years, the Chang 7 member shale has drawn much attention, especially the C7-3SM shale has been regarded as an integrated whole to compared with marine shale [4, 15]. Because in this period, the basin's area and the water body's depth reached the peak [16]. However, the C7-2SM and C9Ms shale were neglected. The deposition time of C7-2SM and C7-3SM is similar. Due to changes in the sedimentary environment, they show significant differences in their shale quality. In the C9M sedimentary period, the lake basin development was still in the

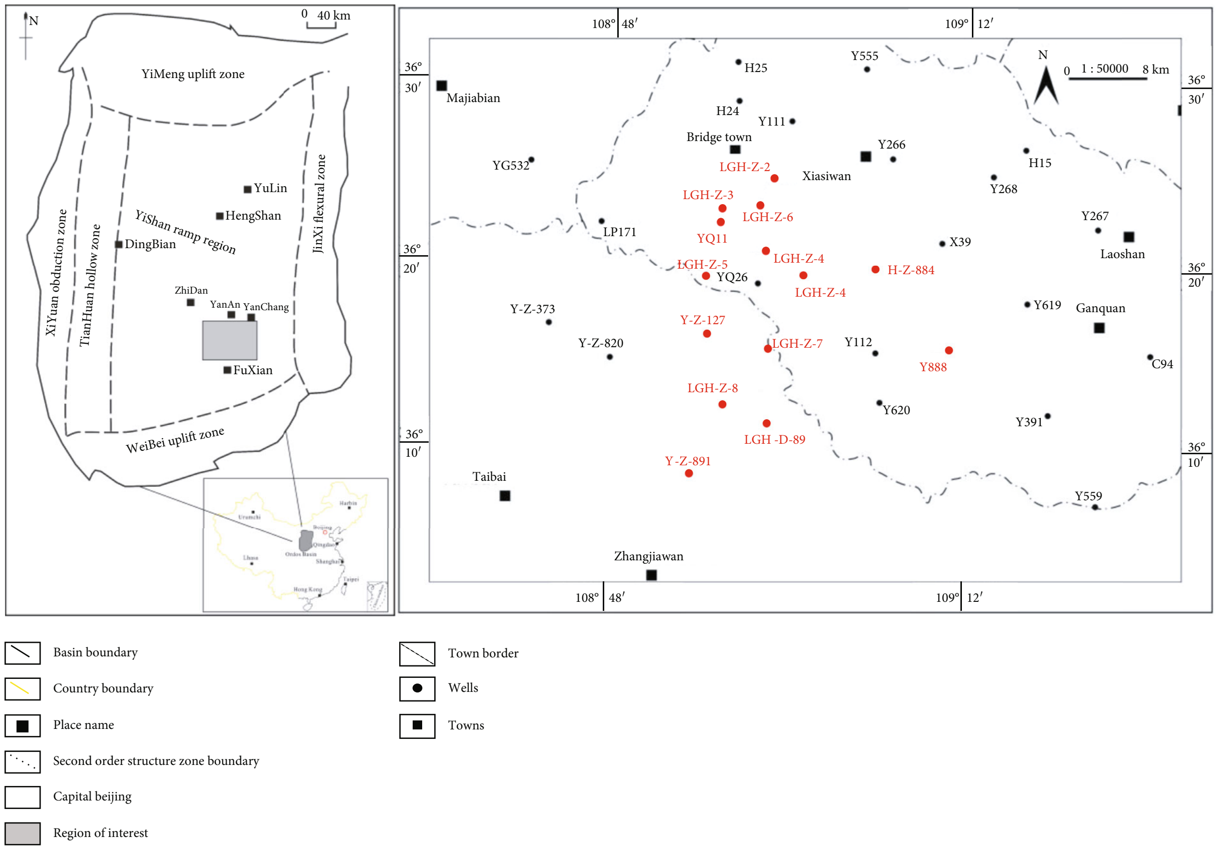

FIGURE 1: Location map showing the research area and drilling cores in the Ordos Basin, Central China.

early stage, which was a semideep lake sedimentary environment [17]. Both Chang 7 and C9Ms shale had similar compositions, with abundant type II organic matter and major minerals such as quartz, clay minerals, and feldspars [15, 18]. They are generally less mature than the marine shale, and the relatively larger amount of clay minerals in Chang 7 and C9M shale affects the methane sorption of bulk rocks under dried conditions [15]. Comprehensively comparative research about different layers of Yanchang Formation shale is much imperative. Based on the previous work [19], the latest research results of Chang 9, systematically comparing C7-2SM, C7-3SM, and Chang 9, were presented in this research.

2. Geological Setting

The Ordos Basin, as one of the most petroliferous and gas-bearing lacustrine basin, is located in the central part of North China [11, 20]. Because of the wrench movement around the basin in the Cenozoic era, the Ordos Basin is now an asymmetric huge north-south syncline with a wide-gentle east limb and a narrow-abrupt west one. The Ordos Basin can be divided into six tectonic units [21, 22], namely, the Northern Yimeng uplift, south Weibei uplift, eastern Jinxi flexural zone, western Xiyuan obduction zone with Tianhuan hollow zone closely next to it, and Yishan ramp region in the center. Yishan ramp region is the main part of the wide-gentle east limb. The research area is located in the southeast of Yishan ramp region and is a western-leaning monocline with lower stratigraphic dip (<1°), gentle average slope (7-8 m/km), and simple internal structure (Figure 1).

The Triassic strata consist of fluvial and lacustrine deposits [23]. The Yanchang Formation was deposited in the late Triassic age and is divided into 10 members from top to bottom according to marker beds and sedimentary cycles. The seismites were widely developed in the whole Yanchang Formation [22], but the shale layers, as the main source rock in the area, were primarily deposited in the Chang 7 and C9Ms (Figure 2). The C9M formed in the early stage of the late Triassic, and the shale layers only occurred in the upper part and mainly consist of lacustrine organic-rich black shale (commonly known as "Lijiatan" shale in China) [24]. The Chang 7 member developed in the period of flooding lake in Ordos Basin. The shale layers, as the main body of Chang 7 member, mostly consist of organic-rich black shale and oil shale (commonly known as "Zhangjiatan" black shale in China) [25].

The Yanchang Formation shale (shale in Chang 9 and Chang 7 members) was deposited in a freshwater lacustrine sedimentary environment, developing obvious organic matter lamina, pyrite framboids, and nanofossils [26, 27]. The Yanchang Formation shale strata is about 80 m thick in average with the thickest area about 100 m, and is now buried in

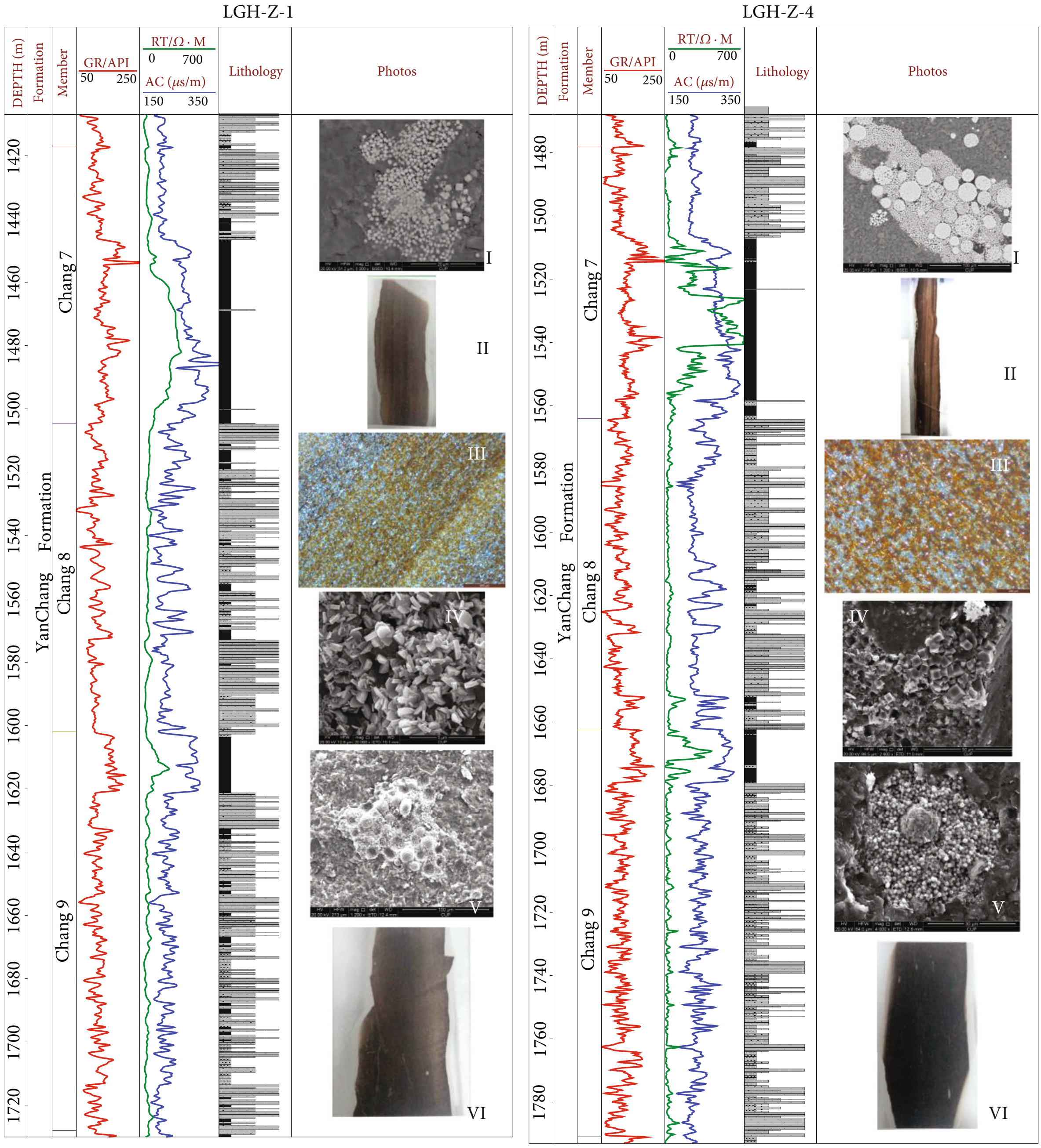

Figure 2: Lithological and logging characteristics of the Yanchang Formation shale in the study area. The photos column: (I) pyrite framboids aggregate in Chang 7 member shale; (II) rock thin sections of Chang 7 member; (III) microscopic photos of rock thin sections; (IV) barites; (V) pyrite framboids in C9M shale; and (VI) rock thin sections of C9M.

depth ranging from 832 m-1700 m with the average of 1288 m. Lamina mainly develops in Chang 7 member shale indicating stronger anisotropy than C9M shale (Figure 2). Pyrite framboids in C9M shale grow separately rather than gathering to aggregate (Figure 2). Heavy minerals, such as barite and phosphorite, can be observed occasionally both in Chang 7 and C9M shale (Figure 2). The organic-rich shales in the Chang 7 member of the Yanchang Formation are self-generation and self-accumulation production systems with oil in fine-grained sedimentary rocks [28].

The Chang 7 member can be divided into three submembers (SM) according to the sedimentary cycle [25, 29]. The lithology of Chang 7-1 SM mainly consists of sandstone and siltstone, which do not belong to the section of Chang 7 member shale reservoir. The Chang 7 member shale can be divided into C7-2SM and C7-3SM (Figure 2). The two SM shale appears to be similar in the gamma readings, with upper possessing relatively higher gamma value as a result of containing volcanic debris with radioactive substances [30] but display a significant difference in the acoustic time

Table 1: Statistical table of samples numbers corresponding to experimental methods.

Experimental methods	C7-2SM	C7-3SM	C9M
XRD	25	17	18
Trace element analysis	25	15	20
TOC and ROCK-EVAL.II methodology analysis	96	29	31
Vitrinite reflectance values	40	13	17

Note: "TOC, ROCK-EVAL.II analysis" means the sample from same depth was used in all the three experiments.

data, with C7-2SM presenting low frustration in AC data and C7-3SM displaying relatively higher and increasing AC values with progressive burial depth.

3. Samples Preparation and Experimental Methods

3.1. Samples Preparation. A series of experiments were conducted, including X-ray diffraction, total organic carbon analysis, rock pyrolysis, and vitrinite reflectance. Shale samples of the C7-2SM, C7-3SM, and C9M cannot be acquired from any individual well so far. The shale sample numbers for each and matching experimental method are presented in detailed in Table 1.

3.2. Experimental Methods

3.2.1. X-Ray Diffraction Analysis and Scanning Electron Microscope Observation. A total of 60 shale samples from Chang 7 and C9M shales were ground to powder finer than 200 mesh (i.e., <75 μm) and then analyzed for whole-bulk and clay fraction (<2 mm) mineralogy by quantitative X-ray diffraction (XRD) analysis by Rigaku automated powder diffractometer (D/MAX-RA) equipped with a Cu X-ray source (40 Kv, 35 mA), following the two independent processes of the CPSC procedure [31]. First, the bulk mineral composition of the powder sample was determined over an angular range of 4-70°2θ at a scanning speed of 1°2θ/min. Second, the clay mineral content was determined over an angular variations of 3-65°2θ at a scanning speed of 1.5°2θ/min after the clay fractions being separated from the rock powder sample. The scanning electron microscope (SEM) observation was also conducted using a Leica microscope with a CRAIC Microscope photometer and FEI Quanta-200F apparatus with an energy-dispersive spectrometer (EDS) in the State Key Laboratory of Petroleum Resources and Prospecting (Beijing) to ascertain image analysis of minerals.

3.2.2. Total Organic Carbon and Rock-Eval Analysis. 156 samples were used in TOC and Rock-Eval analysis, using laboratory apparatus LECO TOC (CS-230HC) and the ROCK-EVAL.II methodology, which were conducted in the State Key Laboratory of Petroleum Resources and Prospecting, China University of Petroleum, Beijing. The samples used in TOC measurement were immersed in 5% HCl solution for two days in order to eliminate the carbonate minerals and then dried in a stoving oven at 65°C for 1.5

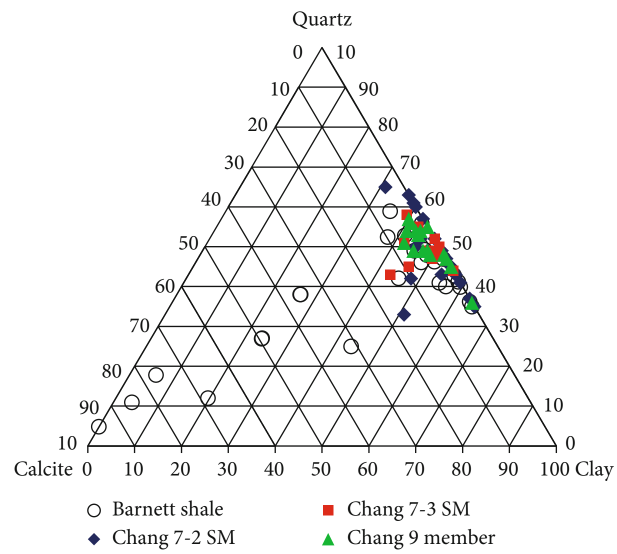

Figure 3: Triangle figure of comparison between terrestrial shale from the Yanchang Formation and Barnett Mineral composition data of Barnett shale samples is from Jarvie et al. [2].

days. Rock-Eval pyrolysis is an established method for characterizing the type and thermal maturity of organic matter in sedimentary rocks as well as their petroleum generation potential [32]. The samples were subjected to programmed heating in an inert atmosphere to determine the amount of volatile gas and residual hydrocarbons (S_1 peak) and the amounts of nonvolatile hydrocarbons and oxygen-containing organic compounds released during thermal cracking of the remaining organic matter in the rock (recorded as S_2).

3.2.3. Vitrinite Reflectance and Trace Element Analysis. The thermal maturity reflected by the experimental vitrinite reflectance values was acquired by full-automatic microscope photometer (MPV-SP). A total of 60 samples were employed for trace element analysis. Samples were crushed into mm-size fragments and washed in 10-percent HCl to leach soluble secondary material (e.g., calcite), followed by agitation in reverse osmosis water prior to powdering. Each sample was heated in 30% H_2O_2 until all organic matter had been digested. The concentration of trace elements in minerals was obtained with laser-ablation microprobe linked with inductively coupled plasma mass spectrometer

Table 2: Mineralogy of 60 Yanchang shale samples.

Number	Depth (m)	Member/SM	Kaolinite	Chlorite	Illite	Illite/smectite mixed layer	Illite/smectite mixed layer ratio	Clay minerals	Quartz	K-feldspar	Plagioclase	Calcite	Dolomite	Pyrite	Siderite
1	1609.95	C7-2SM	0	37	27	36	15	55	30	7	8	0	0	0	0
2	1613.1	C7-2SM	0	31	24	45	15	65	22	7	6	0	0	0	0
3	1620.01	C7-2SM	0	10	31	59	15	31	31	7	12	0	4	15	0
4	1201.47	C7-2SM	0	29	28	43	15	48	36	8	8	0	0	0	0
5	1203.47	C7-2SM	0	18	28	54	15	54	29	8	6	0	3	0	0
6	1209.42	C7-2SM	0	19	26	55	15	51	33	7	9	0	0	0	0
7	1212.53	C7-2SM	0	13	29	58	15	40	28	8	19	0	0	2	3
8	1451.1	C7-2SM	10	16	25	49	15	57	27	5	6	0	0	5	0
9	1452.37	C7-2SM	16	18	36	30	15	57	26	5	9	0	0	3	0
10	1454.42	C7-2SM	9	10	26	55	15	63	23	7	7	0	0	0	0
11	1455	C7-2SM	0	23	24	53	15	48	28	5	7	10	0	2	0
12	1457.04	C7-2SM	0	19	24	57	20	56	29	7	5	0	0	0	3
13	1139.1	C7-2SM	0	8	12	80	15	53	30	7	8	0	0	2	0
14	1145.2	C7-2SM	49	3	11	37	20	48	37	2	8	0	3	0	2
15	1146.16	C7-2SM	4	3	18	75	20	45	36	2	10	0	3	0	4
16	1152.35	C7-2SM	10	13	21	56	15	57	30	7	6	0	0	0	0
17	1155.45	C7-2SM	15	16	22	47	15	39	29	6	9	0	0	17	0
18	1443.77	C7-2SM	0	17	26	57	15	51	26	3	4	0	16	0	0
19	1446.15	C7-2SM	0	16	27	57	15	43	35	8	10	0	0	4	0
20	1447.28	C7-2SM	0	23	24	53	20	45	31	9	6	5	0	4	0
21	1449.49	C7-2SM	0	12	26	62	15	37	31	7	9	0	0	16	0
22	1511.17	C7-2SM	0	14	29	57	15	59	23	5	8	0	0	5	0
23	1516.86	C7-2SM	0	18	21	61	15	56	30	6	8	0	0	0	0
24	1518.62	C7-2SM	0	25	25	50	15	55	29	6	10	0	0	0	0
25	1519.55	C7-2SM	0	25	23	52	15	51	30	6	5	0	0	8	0
26	1608.98	C7-3SM	9	2	21	68	15	44	18	0	4	3	0	0	31
27	1609.18	C7-3SM	9	4	22	65	15	51	22	4	10	1	0	0	12
28	1611.42	C7-3SM	7	7	24	62	15	50	22	3	14	1	0	1	9
29	1611.46	C7-3SM	8	8	17	67	15	50	18	3	7	1	0	8	13
30	1613.08	C7-3SM	4	5	23	68	15	50	22	0	8	3	0	2	15
31	1613.68	C7-3SM	0	10	22	68	15	50	30	0	8	3	0	1	8
32	1619.02	C7-3SM	1	2	18	79	15	42	13	1	12	1	6	22	3
33	1620.38	C7-3SM	0	5	21	74	15	49	25	2	15	2	0	4	3
34	1621.45	C7-3SM	2	4	21	73	15	39	28	3	17	3	0	2	8
35	1386.54	C7-3SM	0	4	20	76	15	43	19	4	9	5	9	2	9

Table 2: Continued.

Number	Depth (m)	Member/SM	Kaolinite	Chlorite	Illite	Illite/smectite mixed layer	Illite/smectite mixed layer ratio	Clay minerals	Quartz	K-feldspar	Plagioclase	Calcite	Dolomite	Pyrite	Siderite
36	1386.58	C7-3SM	0	4	23	73	15	46	20	4	9	6	3	3	9
37	1388.2	C7-3SM	0	7	23	70	15	50	22	5	13	1	0	2	7
38	1392.02	C7-3SM	0	5	24	71	15	48	24	3	14	0	0	0	11
39	1392.46	C7-3SM	0	6	24	70	15	48	27	2	11	3	0	2	7
40	1399.05	C7-3SM	0	7	22	71	15	56	23	2	12	0	0	3	4
41	1399.08	C7-3SM	0	8	22	70	15	50	28	0	16	0	0	2	4
42	1399.37	C7-3SM	0	7	22	71	15	43	25	0	17	2	0	13	0
43	1750.3	C9M	0	11	27	62	15	44	36	3	11	3	0	3	0
44	1755.28	C9M	0	22	30	48	15	53	39	0	6	0	0	2	0
45	1753.25	C9M	0	15	27	58	15	41	30	0	14	0	5	10	0
46	1754.43	C9M	1	1	10	88	15	45	46	0	2	0	6	1	0
47	1360	C9M	0	23	39	38	15	43	42	2	8	0	3	2	0
48	1362.17	C9M	0	18	35	47	15	47	37	0	8	2	2	4	0
49	1364.02	C9M	0	15	18	67	15	44	41	0	12	3	0	0	0
50	1365.15	C9M	0	25	28	47	15	40	47	0	10	3	0	0	0
51	1603.35	C9M	0	17	31	52	15	44	36	2	13	0	2	3	0
52	1603.73	C9M	0	7	25	68	15	42	40	1	9	1	6	1	0
53	1604.16	C9M	0	17	23	60	15	52	29	4	11	0	0	4	0
54	1604.66	C9M	0	16	22	62	15	41	35	4	12	3	0	5	0
55	1597.2	C9M	0	24	32	44	10	49	36	0	8	0	3	4	0
56	1663.39	C9M	0	19	25	56	15	64	23	5	6	0	0	2	0
57	1667.36	C9M	0	15	20	65	15	55	33	0	9	0	0	3	0
58	1668.27	C9M	0	16	25	59	15	48	32	3	11	3	0	3	0
59	1671.39	C9M	0	10	21	69	15	55	32	0	10	0	0	3	0
60	1671.89	C9M	0	15	33	52	15	45	38	0	14	0	0	3	0

Note: SM means submember. Unit of mineral composition is percentage (%). The percentage of types of clay minerals (e.g., kaolinite and illite) is relative to the clay mineral section rather than the whole rock.

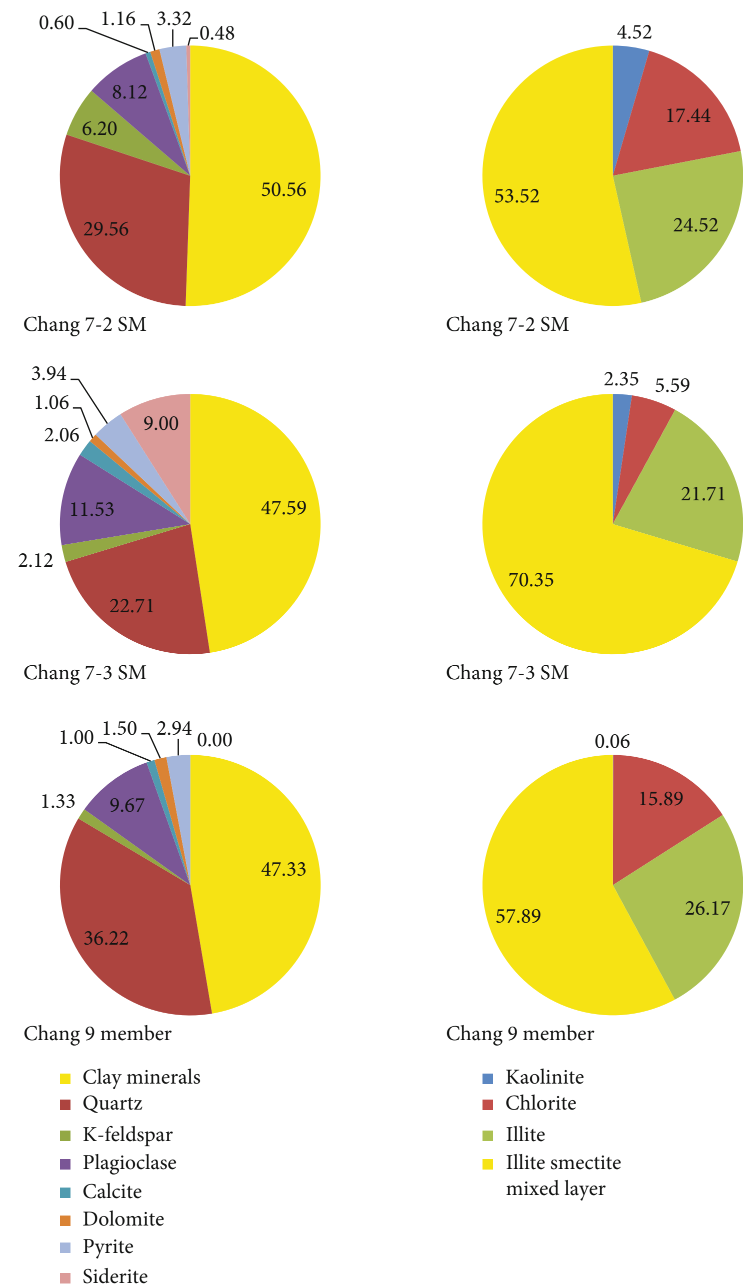

Figure 4: Mineral composition of C7-2SM, C7-3SM, and C9M shale samples.

(LAM–ICP–MS) in the Beijing Research Institute of Uranium Geology, which is the geological experiment research department of the China National Nuclear Corporation (CNNC). Detection limits were typically in the range 100–500 ppb for Sc, 10–100 ppb for Sr, Zr, Ba, Gd, and Pb, 1–10 ppb for Y, Nb, La, Ce, Nd, Sm, Eu, Dy, Er, Yb, Hf, and Ta, and usually 1 ppb for Pr, Th, and U.

3.2.4. Porosity and Permeability Analysis. The cylinder shale samples with a diameter of 2.5 cm and a length of 5 cm for each were analyzed for porosity and permeability in the Reservoir Porous Flow Laboratory of RIPED-Langfang PetroChina. These samples were definitely without factitious microfracture on the surface formed during the drilling process. It is hard to identify artificial microfracture formed in the sample interior before porosity and permeability analysis, which explains aberrant data point appearance.

4. Results

4.1. Mineral Composition and SEM-EDS. There are scarcely any carbonate minerals in both the Chang 7 and C9M shales (Figure 3) compared with the Barnett shale [2, 33]. Illite-smectite mixed layer is the main composition of clay minerals. The C7-2SM exhibits a little bit higher content of clay minerals than the C7-3SM and C9M shale and detrital

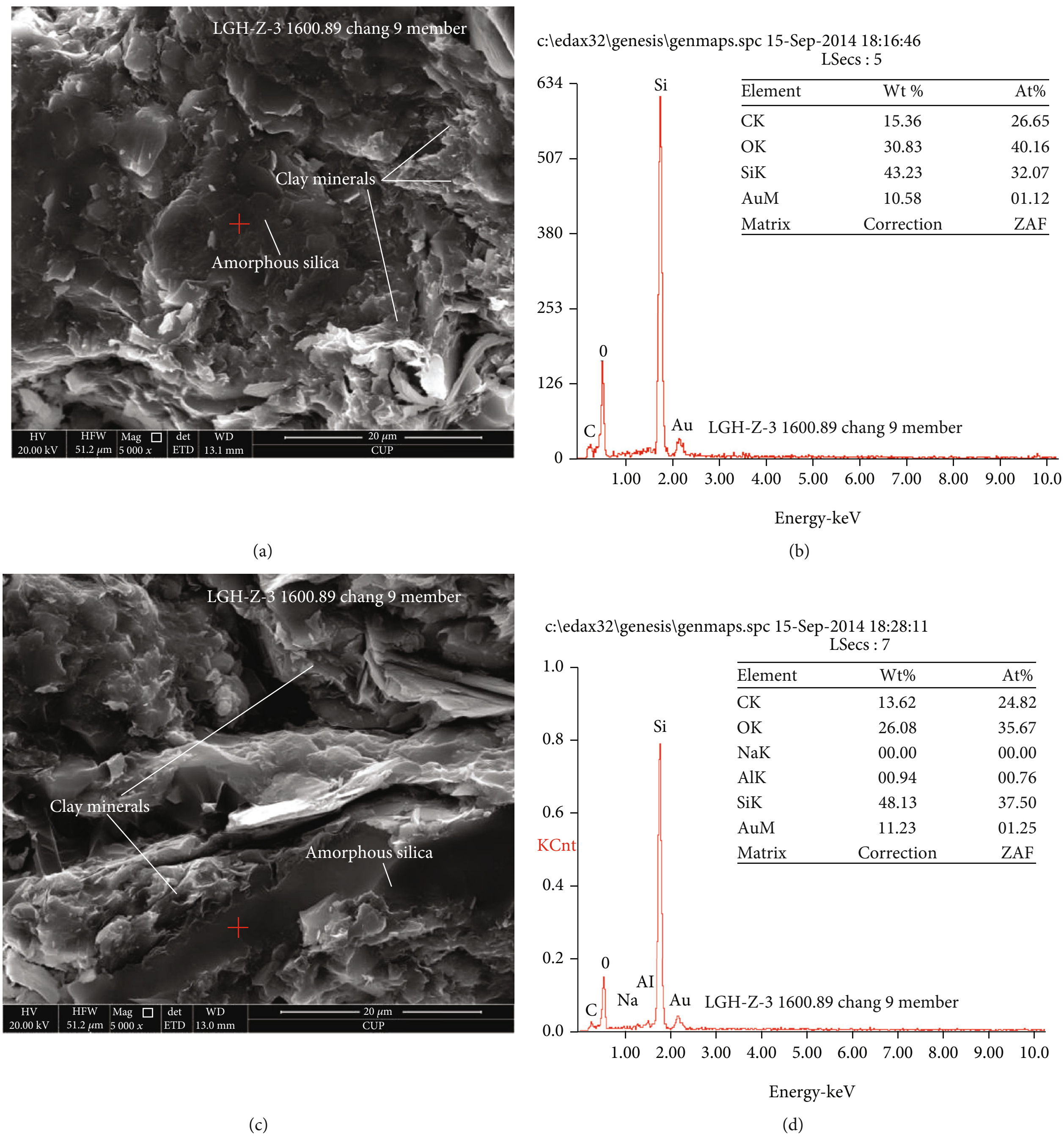

Figure 5: SEM images and EDS of amorphous silica in C7-2SM and C9M shale. The red "+" in the figure is the right point where EDS measures.

minerals (Table 2, Figure 4). The C9M shale owns the highest percentage of quartz (36.22%) and illite (26.17%) while possesses the least amount of K-feldspar (1.33%) and kaolinite (0.06%) (Figure 4). The C7-3SM shale possesses much larger content of illite/smectite mixed layer and less quantity of quartz, which exhibits great dissimilarity with C7-2SM and C9M shales. In C7-2SM and C9M shales, some amorphous silica was observed, which cannot be measured by XRD (Table 2). They are surrounded tightly by clay minerals, and there is no space for them to grow into authigenic microquartz (Figure 5).

4.2. Geochemical Characteristics

4.2.1. Organic Matter Richness. The TOC data points of the C7-2SM and C9M shales are more scattered, mainly ranging from 2% to 12% (Table 3). Most of the TOC values of the C7-2SM shale distribute in the range of 2%~6% and C9M shale in the range of 4%~8%, while that of the C7-3SM shale is chiefly in the variation range of 4%~6%. The C7-3SM shale possesses the highest content of residual bitumen and oil, as indicated by the largest S_1 values, which are approximately equal between the C7-2SM and C9M shales

Table 3: TOC and Rock-Eval of 156 Yanchang shale samples.

Number	Depth (m)	Member/ SM	TOC (%)	Tmax (°C)	S_1 (mg/g)	S_2 (mg/g)	$S_1 + S_2$ (mg/g)	PI	HC (mg/g)	HI (mg/g)	Number	Depth (m)	Member/ SM	TOC (%)	Tmax (°C)	S_1 (mg/g)	S_2 (mg/g)	$S_1 + S_2$ (mg/g)	PI	HC (mg/g)	HI (mg/g)
1	1609.95	C7-2 SM	5.367	454	1.9	7.85	9.75	0.1949	35	146	79	1446.7	C7-2SM	7.147	455	3.66	12.88	16.54	0.2213	51	180
2	1611	C7-2SM	5.393	456	2.01	8.13	10.14	0.1982	37	151	80	1447.28	C7-2SM	6.055	453	3.01	9.61	12.62	0.2385	50	159
3	1612.18	C7-2SM	3.517	453	1.35	5.04	6.39	0.2113	38	143	81	1447.78	C7-2SM	6.067	452	2.87	9.53	12.4	0.2315	47	157
4	1613.1	C7-2SM	4.573	457	2.08	6.84	8.92	0.2332	45	150	82	1448.42	C7-2SM	3.83	454	3.24	6.68	9.92	0.3266	85	174
5	1613.94	C7-2SM	7.139	456	4.24	12.58	16.82	0.2521	59	176	83	1448.96	C7-2SM	4.338	451	2.86	6.97	9.83	0.2909	66	161
6	1615.1	C7-2SM	4.736	447	3.21	8.94	12.15	0.2642	68	189	84	1449.49	C7-2SM	4.794	441	3.38	5.76	9.14	0.3698	71	120
7	1616.18	C7-2SM	6.625	452	4.06	13.15	17.21	0.2359	61	198	85	1450.02	C7-2SM	5.177	451	3.09	6.63	9.72	0.3179	60	128
8	1617.05	C7-2SM	5.977	456	3.78	10.78	14.56	0.2596	63	180	86	1451.04	C7-2SM	5.154	453	2.63	7.77	10.4	0.2529	51	151
9	1618.15	C7-2SM	4.999	452	3.04	8.97	12.01	0.2531	61	179	87	1511.17	C7-2SM	5.758	448	6.03	10.39	16.42	0.3672	105	180
10	1619.2	C7-2SM	5.134	440	4.32	8.79	13.11	0.3295	84	171	88	1512.02	C7-2SM	5.069	448	6.49	11.39	17.88	0.3630	128	225
11	1620.1	C7-2SM	8.773	455	5.18	15.43	20.61	0.2513	59	176	89	1512.94	C7-2SM	4.644	450	4.18	7.51	11.69	0.3576	90	162
12	1621.15	C7-2SM	3.77	450	3.72	8.19	11.91	0.3123	99	217	90	1513.96	C7-2SM	5.49	456	3.53	9.85	13.38	0.2638	64	179
13	1622.17	C7-2SM	10.29	452	4.38	16.97	21.35	0.2052	43	165	91	1514.97	C7-2SM	5.302	453	4.44	10.82	15.26	0.2910	84	204
14	1623.22	C7-2SM	11.41	453	4.58	15.25	19.83	0.2310	40	134	92	1515.92	C7-2SM	3.397	452	3.21	7.36	10.57	0.3037	94	217
15	1624.29	C7-2SM	7.809	450	3.04	10.78	13.82	0.2200	39	138	93	1516.86	C7-2SM	5.11	453	3.73	9.53	13.26	0.2813	73	186
16	1625.24	C7-2SM	11.44	449	3.67	12.42	16.09	0.2281	32	109	94	1517.72	C7-2SM	4.891	453	3.66	8.94	12.6	0.2905	75	183
17	1194.39	C7-2SM	4.101	449	3.29	7.1	10.39	0.3167	80	173	95	1518.68	C7-2SM	4.617	453	3.67	8.81	12.48	0.2941	79	191
18	1195.29	C7-2SM	4.263	456	3	7.2	10.2	0.2941	70	169	96	1519.55	C7-2SM	6.788	456	4.92	13.91	18.83	0.2613	72	205
19	1196.33	C7-2SM	2.433	451	3.69	4.88	8.57	0.4306	152	201	97	1608.08	C7-3SM	6.27	449	7.42	13.99	21.41	0.3466	118	223
20	1197.32	C7-2SM	5.357	456	3.35	9.54	12.89	0.2599	63	178	98	1609.2	C7-3SM	5.15	445	6.88	12.55	19.43	0.3541	134	244
21	1198.34	C7-2SM	4.47	453	3.16	7.75	10.91	0.2896	71	173	99	1611.1	C7-3SM	5.3	447	6.88	12.65	19.53	0.3523	130	239
22	1199.38	C7-2SM	4.539	456	2.98	8.01	10.99	0.2712	66	176	100	1612.15	C7-3SM	5.08	439	8.8	12.37	21.17	0.4157	173	244
23	1200.36	C7-2SM	3.882	452	3.2	7.36	10.56	0.3030	82	190	101	1613.14	C7-3SM	5.39	423	10.24	10.95	21.19	0.4832	190	203
24	1201.47	C7-2SM	4.466	453	2.86	7.41	10.27	0.2785	64	166	102	1614.16	C7-3SM	5.12	443	10.54	15.42	25.96	0.4060	206	301
25	1202.54	C7-2SM	3.014	427	4.51	5.87	10.38	0.4345	150	195	103	1616.2	C7-3SM	6.09	447	9.37	16.05	25.42	0.3686	154	264
26	1203.47	C7-2SM	2.676	419	5.34	5.99	11.33	0.4713	200	224	104	1617.5	C7-3SM	8.81	451	10.87	24.05	34.92	0.3113	123	273
27	1204.45	C7-2SM	5.555	455	4.09	10.43	14.52	0.2817	74	188	105	1618.1	C7-3SM	4.92	444	8.89	14.3	23.19	0.3834	181	291
28	1205.35	C7-2SM	3.914	452	4.4	7.47	11.87	0.3707	112	191	106	1619	C7-3SM	5.26	448	9.04	16.09	25.13	0.3597	172	306
29	1206.44	C7-2SM	5.301	455	4.41	9.51	13.92	0.3168	83	179	107	1620	C7-3SM	1.52	442	3.27	3.04	6.31	0.5182	215	200
30	1207.51	C7-2SM	5.075	451	5.15	9.18	14.33	0.3594	101	181	108	1620.95	C7-3SM	3.29	451	4.73	8.02	12.75	0.3710	144	244
31	1208.5	C7-2SM	4.33	447	5.94	9.06	15	0.3960	137	209	109	1621.55	C7-3SM	3.66	445	5.29	8.09	13.38	0.3954	145	221
32	1209.42	C7-2SM	4.331	450	5.68	9.04	14.72	0.3859	131	209	110	1385.24	C7-3SM	7.32	453	5.19	19.15	24.34	0.2132	71	262
33	1210.58	C7-2SM	4.105	440	6.07	9.43	15.5	0.3916	148	230	111	1386.2	C7-3SM	4.74	450	6.34	10.67	17.01	0.3727	134	225
34	1211.41	C7-2SM	5.245	449	5.32	10.07	15.39	0.3457	101	192	112	1387.12	C7-3SM	5.11	436	5.45	10.19	15.64	0.3485	107	199
35	1212.53	C7-2SM	4.798	454	5.74	10.21	15.95	0.3599	120	213	113	1388.11	C7-3SM	5.45	446	3.77	11.36	15.13	0.2492	69	208
36	1450.2	C7-2SM	5.519	456	2.92	8.22	11.14	0.2621	53	149	114	1389.17	C7-3SM	5.72	448	4.46	13.27	17.73	0.2516	78	232

Table 3: Continued.

Number	Depth (m)	Member/ SM	TOC (%)	Tmax (°C)	S_1 (mg/g)	S_2 (mg/g)	$S_1 + S_2$ (mg/g)	PI	HC (mg/g)	HI (mg/g)	Number	Depth (m)	Member/ SM	TOC (%)	Tmax (°C)	S_1 (mg/g)	S_2 (mg/g)	$S_1 + S_2$ (mg/g)	PI	HC (mg/g)	HI (mg/g)
37	1450.63	C7-2SM	3.911	450	2.79	5.43	8.22	0.3394	71	139	115	1390.17	C7-3SM	5.28	446	4.65	10.96	15.61	0.2979	88	208
38	1451.1	C7-2SM	4.826	453	2.14	6.83	8.97	0.2386	44	142	116	1391.03	C7-3SM	7.16	450	5.79	15.2	20.99	0.2758	81	212
39	1451.23	C7-2SM	3.544	452	1.77	4.67	6.44	0.2748	50	132	117	1391.97	C7-3SM	4.76	443	6.76	11.35	18.11	0.3733	142	238
40	1451.79	C7-2SM	5.293	455	2.82	7.8	10.62	0.2655	53	147	118	1393.06	C7-3SM	5.25	432	6.68	12.36	19.04	0.3508	127	235
41	1452.37	C7-2SM	4.577	452	2.38	6.68	9.06	0.2627	52	146	119	1395.02	C7-3SM	4.51	448	5.34	13.47	18.81	0.2839	118	299
42	1452.78	C7-2SM	3.989	447	2.61	5.09	7.7	0.3390	65	128	120	1394.06	C7-3SM	5.02	451	5.87	14.19	20.06	0.2926	117	283
43	1453.4	C7-2SM	4.274	446	2.62	6.28	8.9	0.2944	61	147	121	1396.02	C7-3SM	4.4	444	5.09	12.53	17.62	0.2889	116	285
44	1453.9	C7-2SM	2.619	436	2.2	3.75	5.95	0.3697	84	143	122	1397.08	C7-3SM	4.87	444	5.59	12.1	17.69	0.3160	115	248
45	1454.42	C7-2SM	4.471	452	2.11	5.47	7.58	0.2784	47	122	123	1398.04	C7-3SM	4.6	455	3.71	11.69	15.4	0.2409	81	254
46	1455	C7-2SM	3.817	447	3.09	5.44	8.53	0.3623	81	143	124	1398.93	C7-3SM	4.99	444	8.54	15.28	23.82	0.3585	171	306
47	1455.33	C7-2SM	4.358	450	2.4	6.13	8.53	0.2814	55	141	125	1400.04	C7-3SM	4.74	431	8.21	11.01	19.22	0.4272	173	232
48	1455.46	C7-2SM	4.319	449	1.95	5.66	7.61	0.2562	45	131	126	1748.3	C9M	6.402	457	3.04	6.93	9.97	0.3049	47	108
49	1455.96	C7-2SM	4.557	450	1.88	5.43	7.31	0.2572	41	119	127	1749.35	C9M	7.004	456	2.88	7.47	10.35	0.2783	41	107
50	1457.04	C7-2SM	5.182	453	3.8	5.77	9.57	0.3971	73	111	128	1750.3	C9M	2.508	458	1.84	7.29	9.13	0.2015	73	291
51	1457.56	C7-2SM	4.365	447	2.05	5.01	7.06	0.2904	47	115	129	1751.3	C9M	6.975	457	1.97	7.27	9.24	0.2132	28	104
52	1457.92	C7-2SM	2.328	418	3.32	3.98	7.3	0.4548	143	171	130	1752.4	C9M	6.309	458	2.43	5.29	7.72	0.3148	39	84
53	1458.51	C7-2SM	3.009	436	2.94	4.15	7.09	0.4147	98	138	131	1753.25	C9M	6.101	458	2.97	6.26	9.23	0.3218	49	103
54	1139.13	C7-2SM	2.433	423	2.83	3.97	6.8	0.4162	116	163	132	1754.43	C9M	1.076	341	2.97	2.71	5.68	0.5229	276	252
55	1140.13	C7-2SM	3.423	448	3.88	6.39	10.27	0.3778	113	187	133	1755.28	C9M	5.443	456	2.84	6.57	9.41	0.3018	52	121
56	1141.16	C7-2SM	0.2747	522	0.38	0.34	0.72	0.5278	138	124	134	1756.33	C9M	4.095	456	1.38	5.8	7.18	0.1922	34	142
57	1141.97	C7-2SM	3.091	447	4.38	4.7	9.08	0.4824	142	152	135	1360.08	C9M	6.007	345	1.99	5.51	7.5	0.2653	33	92
58	1143.17	C7-2SM	5.35	449	4.89	12.8	17.69	0.2764	91	239	136	1361.15	C9M	4.43	455	3	7	10	0.3000	68	158
59	1144.09	C7-2SM	2.904	446	4.27	7.41	11.68	0.3656	147	255	137	1362.17	C9M	10.22	461	5.65	18.18	23.83	0.2371	55	178
60	1145.15	C7-2SM	5.241	449	5.8	14.12	19.92	0.2912	111	269	138	1363.09	C9M	5.281	453	3.76	9.12	12.88	0.2919	71	173
61	1146.25	C7-2SM	2.775	457	5.01	5.34	10.35	0.4841	181	192	139	1364.02	C9M	5.204	453	3.17	9.32	12.49	0.2538	61	179
62	1148.21	C7-2SM	4.941	449	6.77	8.09	14.86	0.4556	137	164	140	1603.35	C9M	6.86	461	2.16	5.55	7.71	0.2802	31	81
63	1149.24	C7-2SM	4.045	455	6.61	8.23	14.84	0.4454	163	203	141	1603.73	C9M	2.924	454	1.77	3.13	4.9	0.3612	61	107
64	1150.31	C7-2SM	3.721	444	5.99	8.11	14.1	0.4248	161	218	142	1604.16	C9M	5.632	452	4.31	10.55	14.86	0.2900	77	187
65	1151.43	C7-2SM	4.176	450	4.99	7.65	12.64	0.3948	119	183	143	1604.66	C9M	5.435	454	4.39	9.35	13.74	0.3195	81	172
66	1152.32	C7-2SM	4.917	453	5.83	8.11	13.94	0.4182	119	165	144	1597.2	C9M	4.769	453	4.68	7.2	11.88	0.3939	98	151
67	1153.41	C7-2SM	3.686	453	4.7	6.09	10.79	0.4356	128	165	145	1598.1	C9M	3.267	446	3.98	6.99	10.97	0.3628	122	214
68	1154.35	C7-2SM	4.084	455	3.52	5.77	9.29	0.3789	86	141	146	1663.39	C9M	5.419	458	2.56	10.55	13.11	0.1953	47	195
69	1155.43	C7-2SM	3.867	460	3.37	5.03	8.4	0.4012	87	130	147	1664.4	C9M	5.995	457	5.7	10.98	16.68	0.3417	95	183
70	1156.33	C7-2SM	2.778	436	3.29	5.2	8.49	0.3875	118	187	148	1665.42	C9M	10.34	462	5.48	12.85	18.33	0.2990	53	124
71	1441.9	C7-2SM	1.461	462	0.85	1.59	2.44	0.3484	58	109	149	1666.44	C9M	4.385	457	4.82	9.04	13.86	0.3478	110	206
72	1442.45	C7-2SM	5.329	458	1.4	7.83	9.23	0.1517	26	147	150	1667.44	C9M	7.165	457	4.94	11.82	16.76	0.2947	69	165

Table 3: Continued.

Number	Depth (m)	Member/SM	TOC (%)	Tmax (°C)	S_1 (mg/g)	S_2 (mg/g)	$S_1 + S_2$ (mg/g)	PI	HC (mg/g)	HI (mg/g)	Number	Depth (m)	Member/SM	TOC (%)	Tmax (°C)	S_1 (mg/g)	S_2 (mg/g)	$S_1 + S_2$ (mg/g)	PI	HC (mg/g)	HI (mg/g)
73	1443.77	C7-2SM	2.144	425	2.28	4.74	7.02	0.3248	106	221	151	1668.25	C9M	6.71	456	4.56	10.85	15.41	0.2959	68	162
74	1444.32	C7-2SM	3.853	455	2.48	5.48	7.96	0.3116	64	142	152	1669.15	C9M	6.308	459	1.73	4.22	5.95	0.2908	27	67
75	1444.79	C7-2SM	4.961	459	2.35	7.42	9.77	0.2405	47	150	153	1669.97	C9M	5.809	455	4.39	9.42	13.81	0.3179	76	162
76	1445.46	C7-2SM	4.142	456	2.53	6.39	8.92	0.2836	61	154	154	1670.9	C9M	6.447	456	4.72	9.33	14.05	0.3359	73	145
77	1445.68	C7-2SM	5.571	457	2.97	10.16	13.13	0.2262	53	182	155	1671.32	C9M	5.287	457	5.3	8.28	13.58	0.3903	100	157
78	1446.15	C7-2SM	7.658	457	3.57	12.96	16.53	0.2160	47	169	156	1671.8	C9M	6.116	452	5.06	9.11	14.17	0.3571	83	149

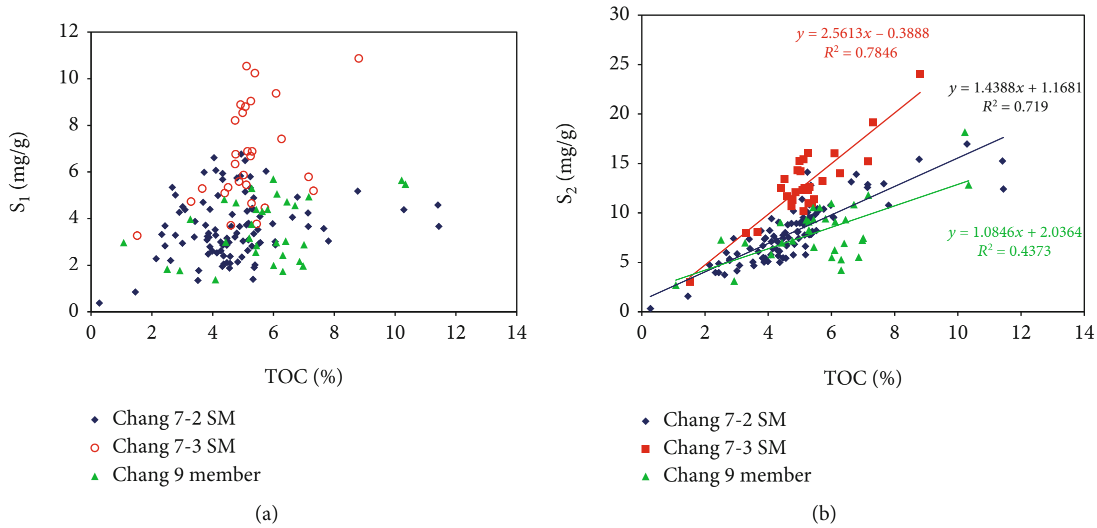

Figure 6: Relationship for C7-2SM, C7-3SM, and C9M shale between S_1, S_2, and TOC.

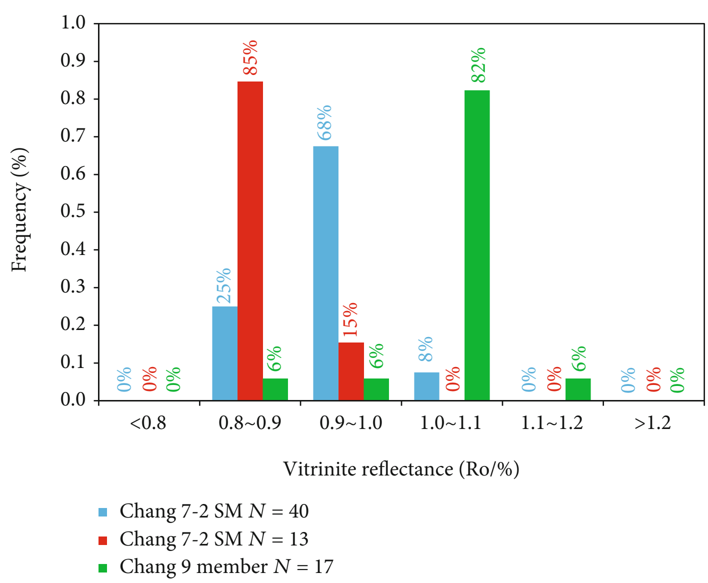

Figure 7: Frequency histogram of Ro for C7-2SM, C7-3SM and C9M shales.

(Figure 6(a)). The TOC of both the Chang 7 and Chang 9 shales exhibits good positive correlation with S_2 values. But the slope value of the line on behalf of the C7-3SM shale is much higher than the other two sections of shale (Figure 6(b)). According to the principle of laboratory apparatus LECO TOC (CS-230HC) analysis, TOC includes the contribution from kerogen and residual bitumen and oil. The C7-3SM shale possesses the highest content of residual hydrocarbon and kerogen.

4.2.2. Organic Matter Maturity. Both the Chang 7 and C9M shales are mainly in the oil window at the present time with R_o ranging from 0.8% to 1.2% (Figure 7, Table 4). S_2 standing for hydrocarbon newly generated during the Rock-Eval process has better positive correlation with TOC than S_1 representing residual hydrocarbon in shale samples, which indirectly indicates the relatively low thermal maturity. Exquisitely compared with each other, the organic matter in Chang 9 shale exhibits the highest thermal maturity, and that in the C7-3SM shale samples the lowest. The C9M shale is buried about 100 m deeper than the Chang 7 member shale, which makes the highest thermal maturity easily understandable. However, the thermal maturity of C7-3SM shale is lower despite being buried deeper than C7-2SM shale, which implies the existence of other controls on thermal maturity.

4.2.3. Organic Matter Types. According to Rock-Eval data, kerogen in both C7-2SM and C9M shales contains mainly type II_2 and possibly type III, especially for C9M shale (Figure 8). Approximately half of the C7-3SM shale samples show the type II_1 kerogen, but the other half of the samples

Table 4: Vitrinite reflectance values of 70 Yanchang shale samples.

Number	Depth (m)	Member/SM	Vitrinite reflectance values (R_o %)	Measuring points	Standard deviation	Number	Depth (m)	Member/SM	Vitrinite reflectance values (R_o %)	Measuring points	Standard deviation
1	1450.2	C7-2SM	0.923	20	0.135	36	1449.49	C7-2SM	0.978	20	0.139
2	1451.1	C7-2SM	0.923	11	0.121	37	1612.18	C7-2SM	0.958	22	0.132
3	1452.07	C7-2SM	0.926	24	0.144	38	1613.94	C7-2SM	0.975	22	0.15
4	1453.4	C7-2SM	0.92	25	0.112	39	1618.15	C7-2SM	0.969	21	0.091
5	1454.42	C7-2SM	0.93	24	0.097	40	1622.17	C7-2SM	0.979	15	0.176
6	1456.6	C7-2SM	0.924	21	0.142	41	1605.33	C7-3SM	0.855	31	0.131
7	1458.51	C7-2SM	0.923	20	0.083	42	1607.3	C7-3SM	0.853	29	0.118
8	1139.1	C7-2SM	0.835	19	0.088	43	1609.7	C7-3SM	0.857	31	0.128
9	1142.09	C7-2SM	0.839	17	0.09	44	1611.45	C7-3SM	0.864	29	0.127
10	1146.16	C7-2SM	0.84	25	0.118	45	1613.59	C7-3SM	0.883	25	0.107
11	1150.25	C7-2SM	0.845	24	0.094	46	1616.75	C7-3SM	0.827	21	0.134
12	1153.35	C7-2SM	0.843	22	0.086	47	1622.8	C7-3SM	0.911	24	0.147
13	1156.45	C7-2SM	0.848	12	0.127	48	1388.97	C7-3SM	0.843	24	0.145
14	1442.45	C7-2SM	0.915	25	0.093	49	1391.3	C7-3SM	0.87	3	0.108
15	1445.46	C7-2SM	0.913	15	0.102	50	1393.25	C7-3SM	0.879	13	0.169
16	1447.78	C7-2SM	0.924	20	0.085	51	1396.37	C7-3SM	0.883	16	0.084
17	1451.04	C7-2SM	0.931	28	0.107	52	1397.56	C7-3SM	0.891	18	0.142
18	1511.17	C7-2SM	1.012	12	0.103	53	1400.73	C7-3SM	0.914	9	0.116
19	1515.92	C7-2SM	1.018	25	0.111	54	1603.35	C9M	1.066	14	0.081
20	1519.55	C7-2SM	1.019	25	0.145	55	1604.42	C9M	1.063	19	0.139
21	1195.29	C7-2SM	0.854	13	0.076	56	1603.73	C9M	1.042	23	0.096
22	1202.54	C7-2SM	0.855	16	0.135	57	1599.05	C9M	1.074	17	0.134
23	1206.44	C7-2SM	0.86	32	0.145	58	1603.12	C9M	1.094	16	0.114
24	1212.53	C7-2SM	0.864	20	0.085	59	1597.2	C9M	1.046	10	0.107
25	1609.95	C7-2SM	0.943	16	0.142	60	1602.1	C9M	1.062	15	0.093
26	1616.18	C7-2SM	0.955	15	0.081	61	1604.98	C9M	1.062	15	0.093
27	1620.1	C7-2SM	0.96	22	0.086	62	1663.39	C9M	1.09	20	0.097
28	1624.29	C7-2SM	0.976	13	0.11	63	1668.27	C9M	1.095	13	0.104
29	1450.74	C7-2SM	0.941	17	0.093	64	1671.89	C9M	1.102	25	0.174
30	1452.78	C7-2SM	0.965	18	0.065	65	1361.15	C9M	0.889	10	0.095
31	1455.5	C7-2SM	0.969	21	0.088	66	1748.3	C9M	0.984	13	0.081
32	1457.56	C7-2SM	0.971	17	0.081	67	1752.4	C9M	1.012	25	0.157
33	1441.9	C7-2SM	0.949	10	0.091	68	1756.33	C9M	1.016	22	0.146
34	1443.77	C7-2SM	0.976	10	0.073	69	1750.3	C9M	1.094	28	0.107
35	1446.7	C7-2SM	0.972	21	0.126	70	1754.43	C9M	1.097	3	0.27

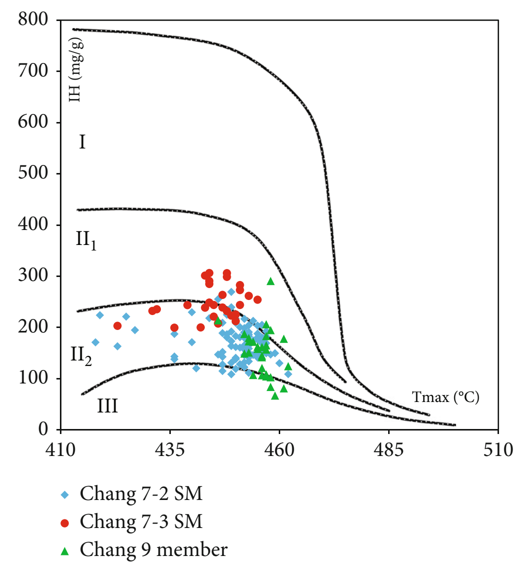

FIGURE 8: Plot of hydrogen index (HI) versus Tmax, showing the types of organic matter for C7-2SM, C7-3SM, and C9M shales.

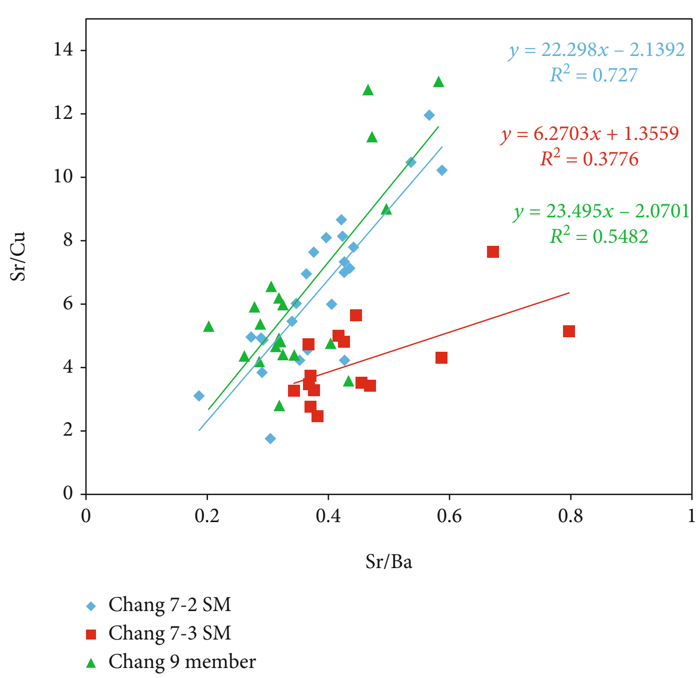

FIGURE 9: The relationship between Sr/Ba and Sr/Cu. The C7-3SM shale exhibits special linear correlation between Sr/Ba and Sr/Cu.

present the type II_2 kerogen, and the data points are distributed a little far away from the type III threshold line (Figure 8). It can be an explanation of possessing the highest values of S_1 and S_2 with medium content of TOC and the lowest thermal maturity.

4.3. Trace Element Analysis. Element B is regarded as a common parameter that possesses a positive linear correlation with salinity of sedimentary water [34, 35]. In Yanchang Formation shale, B was not determined at all, indicating a freshwater sedimentary environment. The Sr/Ba is another parameter sensitively reflecting the salinity of sedimentary water. It represents freshwater sedimentary environment when the Sr/Ba value is less than 1 [36, 37], which is exactly describing the Yanchang Formation shale samples (Figure 9). The Sr/Cu is a parameter employed to express the dry-humid degree of sedimentary environment. It represents warm-moist climate when the Sr/Cu values range from 1 to 10 [34, 37], which is exactly describing most of the Yanchang Formation shale samples.

The dry-humid degree of the sedimentary environment has a great influence on the salinity of sedimentary water. The Yanchang Formation shale presents a linear correlation between Sr/Ba and Sr/Cu (Table 5). The slope value of the

Table 5: Trace element composition of 60 Yanchang shale samples.

Number	Depth (m)	Member/SM	Li	Be	Sc	V	Cr	Co	Ni	Cu	Zn	Ba	La	Ce	Th	U	Sr	Mo
1	1451.1	C7-2SM	59.6	3.44	17.2	95.9	92.4	21.9	58	57.7	118	962	45.3	76.1	10.8	3.33	281	4.42
2	1452.37	C7-2SM	67.3	2.48	14.3	97.8	105	22	47.5	57	103	973	45.6	79.6	11.3	3.26	281	2.77
3	1454.42	C7-2SM	84.7	2.96	18	113	111	18.9	42.8	55.5	114	963	47.3	87.6	11.3	3.17	334	2.16
4	1455	C7-2SM	69.3	3.04	20.5	107	113	19.6	40.9	66.7	133	1071	46.4	80.8	10.5	3.41	364	2.39
5	1457.04	C7-2SM	74.2	2.49	22.4	114	95	21.3	40.4	56.6	110	930	49.5	89.1	10.7	3.86	396	1.6
6	1139.1	C7-2SM	42.8	3.02	15.2	112	114	23.7	62.4	72.4	144	1207	41.6	75	14.6	3.65	225	1.94
7	1145.2	C7-2SM	18.5	4.04	12.7	72.8	75.6	12.5	25.2	33.2	87.3	701	35.8	66.9	17	4.39	397	3.35
8	1146.16	C7-2SM	24.1	2.79	12.9	81.3	87.3	14.8	31.1	43	89.7	878	37.9	68.6	13.3	4.09	348	2.75
9	1152.35	C7-2SM	58.9	2.23	20.2	101	133	18.8	37.3	50.6	112	968	48.4	91.2	10.8	3.78	352	2.62
10	1155.45	C7-2SM	66.1	2.36	22.1	108	105	27.1	58.7	53.5	115	945	49.5	93.3	11.4	3.79	417	6.01
11	1443.77	C7-2SM	21.2	2.61	17	98.7	81.8	9.62	21.6	40.5	90.4	791	36.8	65.5	12.3	4.18	424	0.927
12	1446.15	C7-2SM	46.3	2.24	19	94	99.2	18.7	37.5	79.2	120	951	42.6	76.1	10.6	5.58	335	3.57
13	1447.28	C7-2SM	62.7	2.22	22.1	107	102	22.1	45.3	67.9	116	1004	50.1	88.9	9.9	5.13	407	2.44
14	1449.49	C7-2SM	43.4	1.93	18	102	93.5	21.8	55.2	54.3	101	934	45.5	84	10.5	3.26	398	19
15	1511.17	C7-2SM	36.5	2.96	22	99.3	86.5	16.8	43.4	140	154	809	42.1	75.9	15.6	7.47	246	6.61
16	1516.86	C7-2SM	57	2.4	18.4	109	102	18.8	44.1	49.3	120	858	46	84.9	12.3	3.1	504	1.59
17	1518.62	C7-2SM	64.7	2.48	20.2	95.1	101	19.4	36.5	51.7	116	1051	47.9	90.4	11.9	4.02	395	1.48
18	1519.55	C7-2SM	75	2.68	18.7	124	117	21.5	53.2	61.9	146	820	42.4	75.3	12.7	4.66	238	5.05
19	1609.95	C7-2SM	78.8	2.72	20.6	109	110	21.4	52	66.5	117	1212	51.7	92	13.8	4.1	330	2.98
20	1613.1	C7-2SM	89	2.75	22.5	116	106	24.5	55.3	60.3	134	988	49.8	89.6	12.3	3.77	430	2.34
21	1620.01	C7-2SM	30.8	1.99	16.5	111	92.9	19.4	38	81.1	113	804	31.8	56.3	9.77	10.1	343	7.55
22	1201.47	C7-2SM	64.8	2.34	22.3	114	107	19.5	41.3	53.3	115	1025	55.5	111	11.7	4.78	434	2.51
23	1203.47	C7-2SM	29.2	2.73	29.4	124	87	24.1	52.8	36.5	86.8	750	34.4	66.2	11.4	4.05	316	1.82
24	1209.42	C7-2SM	53.8	2.4	20.2	107	112	21.5	55.1	76.2	136	949	43.3	79.1	11.4	6.29	347	3.71
25	1210.58	C7-2SM	25.8	2.18	17.5	104	87.7	18.7	38.2	56.2	105	974	36.3	67.4	9.97	4.24	341	1.91
26	1608.98	C7-3SM	14.8	1.55	21	99.8	103	13.5	30.8	76.5	88.4	493	49.1	94.3	7.32	4.87	393	1.16
27	1609.18	C7-3SM	49.7	2.12	14.9	101	86.3	15.9	32.1	61.7	107	742	37.7	70.9	9.68	3.09	309	1.14
28	1611.1	C7-3SM	40.8	2.68	15.8	96	124	17.6	35.7	66.4	112	856	44.9	82.9	10.4	3.58	314	1.96
29	1611.42	C7-3SM	63.3	2.33	16.6	111	109	22.3	46.7	99.6	133	869	42.9	83.8	10.5	4.04	327	2.16
30	1611.46	C7-3SM	49.7	2.22	20.5	128	294	20.9	53.3	98.8	127	763	44	85	9.89	4.07	347	5.49
31	1613.08	C7-3SM	40.8	3.2	15.5	93.7	115	19.2	41	87.1	145	641	46.7	93.9	15.9	6.05	376	1.73
32	1613.68	C7-3SM	42.9	2.78	17.5	112	104	19.4	35.6	91.3	126	668	46.7	85.7	14	4.35	313	1.7
33	1620.38	C7-3SM	33	2.48	14.2	105	109	19.5	42.7	65.3	135	737	42.8	77.4	11.6	2.88	314	1.44
34	1621.45	C7-3SM	17.1	1.14	11.2	79.5	67.2	17.4	24.3	58.3	83	664	48.4	89.9	7.63	2.17	446	1.18
35	1386.54	C7-3SM	33.1	1.75	11.8	66.4	66.3	14.4	28.7	92.6	106	938	41.2	75.7	7.63	3.23	347	1.46

Table 5: Continued.

Number	Depth (m)	Member/SM	Li	Be	Sc	V	Cr	Co	Ni	Cu	Zn	Ba	La	Ce	Th	U	Sr	Mo
36	1388.2	C7-3SM	50.6	2.1	16.2	123	121	22.2	54.9	102	151	971	43.1	77.5	10.1	3.29	333	2.59
37	1392.02	C7-3SM	36.4	2.63	16.7	99.3	109	15.7	25.6	86.2	113	814	46.2	83.4	11.3	3.11	299	1.58
38	1392.46	C7-3SM	30.4	2.76	17.3	97	78.6	17	36	53.1	96.9	674	47.5	84.6	14.5	3.97	300	1.8
39	1399.05	C7-3SM	45.3	2.73	14.7	98.4	87.9	18	35.5	108	154	805	43.5	81.1	13	5.08	298	2.54
40	1399.37	C7-3SM	39.9	2.06	12.7	96.7	220	16.9	50	108	128	700	33.3	60.7	9.27	4.66	267	7.66
41	1603.35	C9M	36.8	2.39	16.3	86	95.2	18.1	39.5	103	134	906	44.1	75.4	13.1	4.83	289	3.39
42	1603.73	C9M	17.4	3.08	9.78	48.9	44.3	8.86	18.7	28.9	66.3	691	34.7	58.5	14.1	4.4	326	2.47
43	1604.16	C9M	41	2.49	15.3	89.2	101	19	41.5	52.6	115	1379	44	82	10.8	3.21	279	3.26
44	1604.66	C9M	39	2.03	14.3	75.3	80.9	18.2	40.2	55	97.4	919	40.2	73.7	10.1	3.23	240	2.42
45	1597.2	C9M	37.6	2.49	16.5	92.8	98.2	18.3	43.9	45.9	112	710	38.2	67.6	14.5	3.75	226	4.95
46	1663.39	C9M	56.1	3.27	23.4	117	107	20.6	44.8	68	124	924	41.9	73.1	12.4	4.26	300	1.75
47	1667.36	C9M	33.8	2.76	13.2	79.9	76.4	13.5	29.8	43.6	83.9	936	38.7	67.1	13.9	5.02	286	2.2
48	1668.27	C9M	39.5	2.58	15.5	91.2	80.7	15.5	30.2	50.8	99.8	950	44	78.1	13.9	4.47	273	1.99
49	1671.39	C9M	31	3.09	16.6	102	84.7	18.1	35.7	60.2	109	711	36.8	64.4	13.4	7.01	287	3.92
50	1671.89	C9M	39.6	2.55	23.9	102	114	21	46.1	50.1	112	910	70.5	117	15.6	7.17	451	5.09
51	1753.25	C9M	25.4	2.21	14.2	66.8	66	16.4	34.3	50.2	99.1	977	39.6	71.4	12.5	4.62	311	6.16
52	1750.3	C9M	35.6	2.58	17.2	84.9	89.7	16	35.7	51.9	90.2	1105	46.1	83.8	15.4	4.94	307	3.12
53	1752.4	C9M	24.5	2.49	14.8	77.9	68.3	16.3	35.7	53	93	976	43.9	78	18.1	7.36	317	6.58
54	1749.35	C9M	26.4	2.23	15.8	58.4	65.6	13.1	21.7	33.6	102	922	33	57.2	12.1	3.45	429	1.53
55	1755.28	C9M	42.2	2.81	18.8	107	108	19.4	46.7	57.3	115	840	44.2	79.4	16.9	6.18	240	3.85
56	1748.33	C9M	38	2.31	16.5	96.2	87	18.2	40	59.6	96.9	888	47.7	85.9	13.4	5.95	278	4.46
57	1360	C9M	39.6	2.95	17.5	98.8	194	18.8	42.4	53.9	102	690	36	64.1	14.5	5.04	237	4.95
58	1362.17	C9M	42.2	2.84	18.3	96.2	114	18.4	42.4	55	103	826	46.7	86.1	16.2	4.77	265	2.85
59	1363.09	C9M	32.9	2.52	17.9	138	111	19.3	43.1	73.2	120	605	38.3	67.9	11.9	7.58	262	7.53
60	1365.15	C9M	31.8	1.72	15.1	61	123	10.6	25.3	23.5	72.5	526	31.8	60.3	8.99	2.45	306	1.39

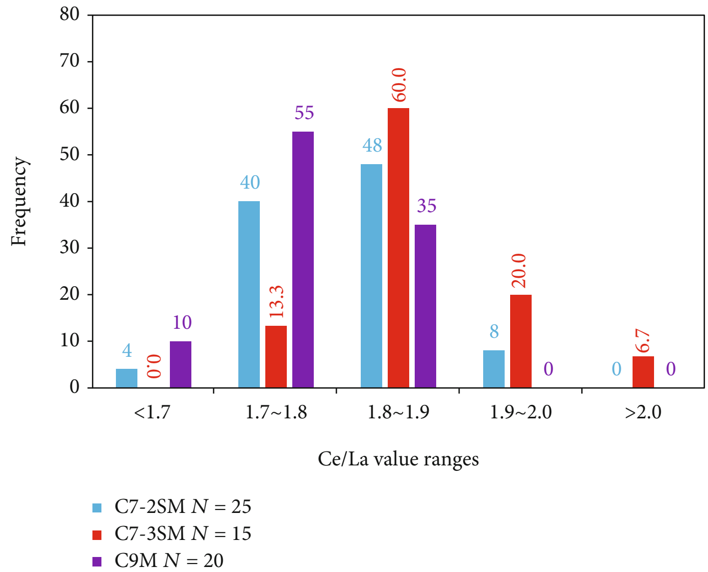

(a)

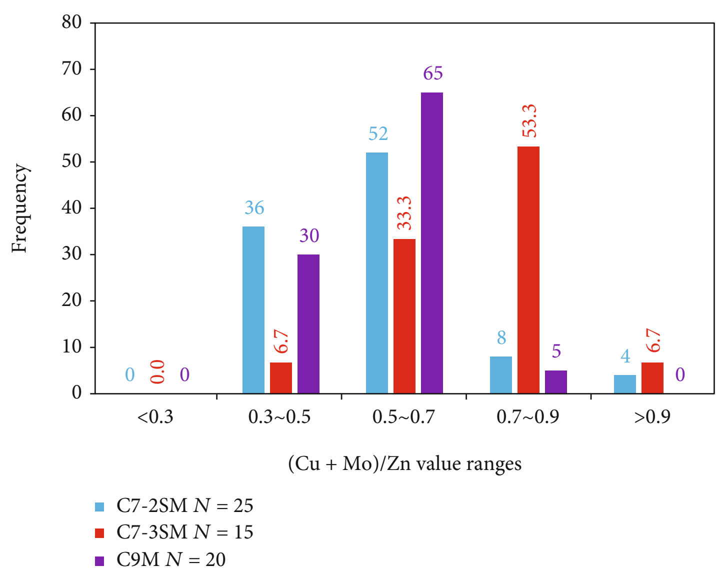

(b)

Figure 10: Continued.

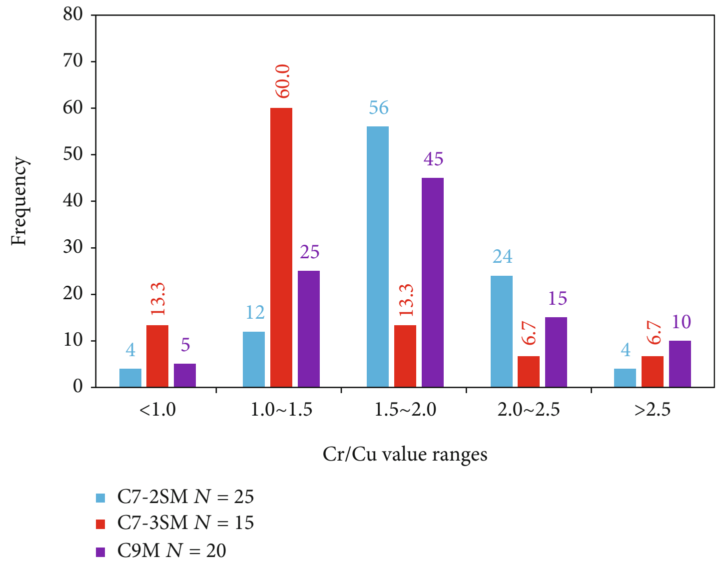

(c)

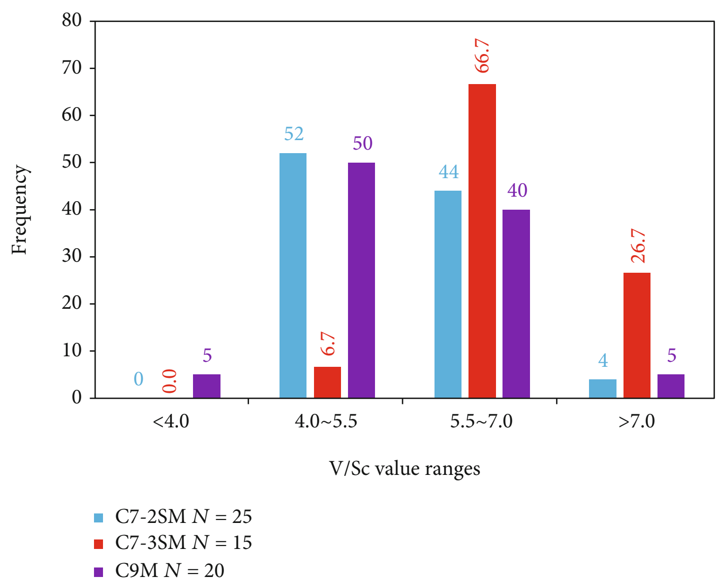

(d)

Figure 10: The resolution comparison of reducing environmental exquisite changes for variety of parameters. The parameters of (Cu+Mo)/Zn and Cr/Cu show higher sensitivity. (Cu+Mo)/Zn and Cr/Cu values are generally much larger and smaller, respectively, for C7-3SM shale.

line on behalf of the C7-3SM shale is much lower than those of the lines representing the C7-2SM shale and C9M shale, which means relatively higher salinity of sedimentary water for the C7-3SM shale (Figure 9).

A large quantity of parameters have been used to reflect the reducibility or oxidability of sedimentary environment, such as Ce/La, Th/U, Cr/V, Cr/Cu, V/Sc, V/(V+Ni), and (Cu+Mo)/Zn [38–41]. All the parameters mentioned above indicate a reduced environment for the Yanchang Formation shale. But only the parameters of Ce/La, (Cu+Mo)/Zn, V/Sc and Cr/Cu satisfy our requirement to exquisite comparison among C7-2SM, C7-3SM and C9M shale (Figure 10). Compared with C7-2SM and C9M shales, the Ce/La, (Cu+Mo)/Zn, and V/Sc values of the C7-3SM shale are much larger and the Cr/Cu values smaller (Figure 11), which represents a stronger reducing environment. It was also indicated indirectly by much larger percentage of reducing minerals, pyrite and siderite, in Figure 4.

4.4. Porosity and Permeability. The Chang 9 member shale possesses the highest porosity followed by the Chang 7-2 SM shale. Although two samples from the Chang 7-3 SM shale display higher permeability, in general, no apparent difference of permeability occurs among the three sections of shale (Table 6).

5. Discussion

Sedimentation and diagenesis are the main controlling factors for the differences among the three members and also

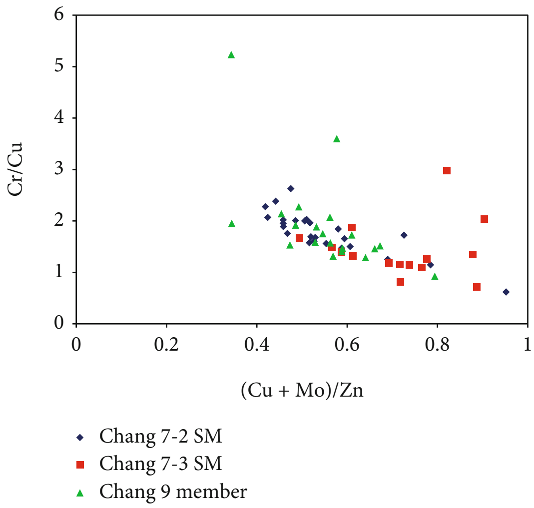

Figure 11: The cross-plot of (Cu+Mo)/Zn and Cr/Cu for C7-2SM, C7-3SM, and C9M shale samples.

lead to the enrichment of organic matter and the potential of oil and gas resources. According to the trace element analysis, the C7-3SM shale developed under much deeper and stratified water. The relatively larger amount of reducing minerals in C7-3SM shale, pyrite and siderite, implies a different sedimentary environment from the C7-2SM and C9M shales. Furthermore, much deeper water represents further away from the sediment provenance, which explains the much larger content of illite/smectite mixed layer and less quantity of quartz.

The C9M shale is buried deeper than Chang 7 member shale and has experienced stronger diagenesis, which explains the nearly disappearance of kaolinite. In addition, more K-feldspar was dissolved for the C9M shale during the burial diagenesis to provide K^+ for smectite-illite transformation, reducing the most amount of illite and the least content of K-feldspar. The smectite to illite reaction is a dissolution–precipitation reaction [42, 43]. This reaction releases locally high silica supersaturation in the pore water, which probably provides silica source for the authigenic microquartz crystals [44, 45]. According to the experiment [46], about 18% of the silica (1101.1 g of the products produced by the reaction, including 197.7 g of silica) will be released during the conversion of montmorillonite to illite. The chemical reaction formula adopted is as follows:

$$\begin{aligned} &1.308\left[(Al_{3.15}Mg_{0.85})(Si_{8.00})O_{20}(OH)_4(Na_{0.85})2H_2O\right.\\ &\quad\left.+\,(0.06Fe_2O_3+0.56K_2O+0.02CaO)\right]\\ &\quad\longrightarrow\left[(Al_{4.12}Fe_{0.1}Mg_{0.56})(Si_{7.17})O_{20}(OH)_4(K_{1.47}Na_{0.01}Ca_{0.03})\right]\\ &\quad+\,3.29SiO_2+0.56Na_2O+0.55MgO+3.23H_2O. \end{aligned} \tag{1}$$

It was another contribution to the larger content of quartz in C9M shale.

In fact, the drilling orientation was the major factor to porosity and permeability. Samples with drilling orientation perpendicular to sedimentary stratification (“vertical” samples) display relatively lower porosity and permeability than samples with drilling orientation parallel to sedimentary stratification (“parallel” samples) because of the existence of lamina, which improves porosity and permeability in the research about the Yanchang Formation shale of Ordos Basin. Regardless of the degree of compaction and diagenesis, the laminar zone, where different mineral zones come into contact with each other, is always the weakest zone in the sample and has gaps that are difficult to close. “Vertical” samples are lack of lamina. Alternatively, the striations developed in the sample are perpendicular to the flow direction of the gas used in the permeability test. In permeability tests, gas is more likely to pass through the gap between the two different laminates. If the laminar is perpendicular to the direction of gas flow, it is equivalent to gas from one medium into another medium, and the flow velocity must be reduced. Lamina is the main contribution to bedding fissure development, which is the key factor to induce cylinder shale samples fragmentation when being drilled perpendicularly to sedimentary stratification.

Besides, porosity displays a positive correlation with the content of quartz, no matter for “vertical” samples or “parallel” samples (Figure 12). Compaction of soft muds to hard shale during progressive burial involves both mechanical and chemical processes causing significant changes of the physical mudstone rock properties. In the shallow parts (<2 km) of sedimentary basins, the sediments compacted mostly mechanically. The Yanchang Formation shale strata is buried in depth ranging from 2730 ft to 5577 ft (832 m-1700 m) with an average of 4225.7 ft (about 1288 m), which means mechanical compaction dominates the changes of shale physical properties. Hence, the special mineral composition of the Chang 7-3 SM, a small percentage of quartz and large quantity of illite/smectite mixed layer, exactly explains the lowest porosity.

6. Conclusion

Based on mineralogical and geochemical characteristics, this work compared C7-2SM, C7-3SM, and Chang 9 shales:

(1) All three section of shales developed in a freshwater sedimentary environment. But the C7-3SM shale samples formed in deeper sedimentary water of relatively higher salinity and stronger reducibility, inducing the largest content of illite/smectite mixed layer and the least quantity of quartz. The C7-2SM and C9M shale formed in similar sedimentary environment according to the trace element characteristic and mineral composition in view of mineral evolution during diagenesis

(2) The C7-3SM shale owns higher S_1 values and productivity of hydrocarbon per gram TOC due to type II_1 kerogen. Kerogen in C7-2SM and C9M shale contain mainly type II_2 and possibly type III, organic matter, especially for C9M shale

Table 6: Porosity and permeability of the Yanchang shale samples.

Number	Depth (m)	Way of drilling	Member/SM	Length (cm)	Diameter (cm)	Porosity (%)	Permeability (mD)
1	1409.31	Vertical	C7-2SM	4.039	2.489	0.646	0.002933
2	1414.15	Vertical	C7-2SM	5.065	2.494	0.400	0.000961
3	1415.67	Vertical	C7-2SM	2.821	2.497	1.385	0.000927
4	1417.73	Vertical	C7-2SM	2.735	2.492	0.964	0.000331
5	1418.95	Vertical	C7-2SM	3.933	2.494	0.857	0.000303
6	1420.88	Vertical	C7-2SM	2.958	2.492	1.331	0.000501
7	1419.66	Parallel	C7-2SM	2.757	2.494	2.229	0.001192
8	1141.92	Parallel	C7-2SM	2.870	2.460	2.690	0.001634
9	1386.12	Parallel	C7-3SM	4.920	2.458	2.262	0.000468
10	1388.72	Parallel	C7-3SM	2.755	2.478	2.062	0.001002
11	1392.62	Parallel	C7-3SM	2.946	2.496	2.779	0.000201
12	1392.77	Parallel	C7-3SM	2.783	2.479	2.375	0.000178
13	1399.25	Parallel	C7-3SM	2.686	2.482	2.585	0.007016
14	1399.78	Parallel	C7-3SM	3.302	2.490	2.976	0.000047
15	1398.37	Parallel	C7-3SM	3.470	2.490	2.118	0.002029
16	1608.28	Parallel	C7-3SM	2.972	2.483	1.341	0.004561
17	1613.38	Parallel	C7-3SM	3.892	2.494	2.030	0.002188
18	1619.22	Parallel	C7-3SM	3.808	2.492	1.631	0.000664
19	1621.85	Parallel	C7-3SM	4.249	2.499	2.135	0.000197
20	1611.12	Vertical	C7-3SM	4.779	2.491	0.786	0.000068
21	1611.86	Vertical	C7-3SM	2.839	2.489	0.615	0.000535
22	1620.68	Parallel	C7-3SM	2.778	2.495	1.962	0.000428
23	1360.75	Parallel	C9M	3.000	2.470	3.790	0.001289
24	1600.19	Parallel	C9M	2.880	2.480	2.550	0.002533
25	1671.34	Parallel	C9M	2.770	2.470	3.330	0.001781

Vertical: drilling orientation perpendicular to sedimentary stratification. Parallel: drilling orientation parallel to sedimentary stratification.

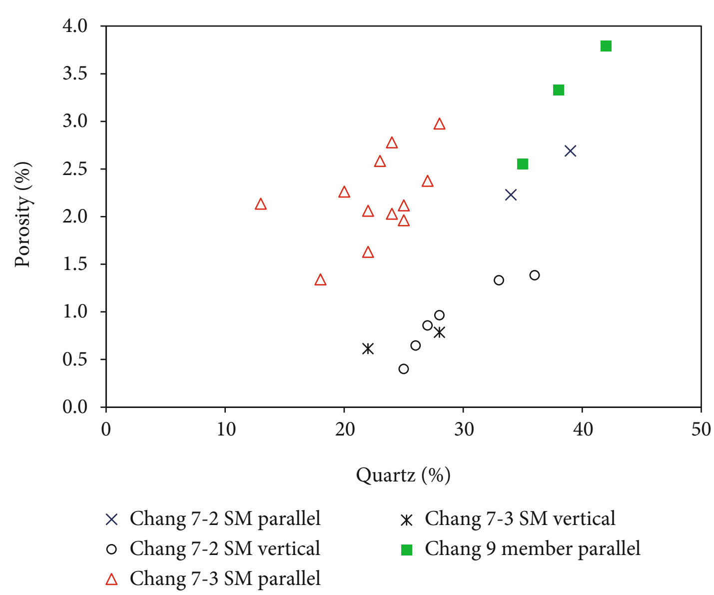

Figure 12: Relationship for the Chang 7-2 SM, Chang 7-3 SM, and Chang 9 member cylinder shale samples between porosity and content of quartz.

(3) The C7-3SM shale samples display the lowest porosity. The drilling orientation and the small content of quartz contributed to the lowest porosity for the C7-3SM shale

Data Availability

The data used to support the findings of this study are included within the article and available from the corresponding author upon request.

Conflicts of Interest

The authors declare that they have no conflicts of interest.

Acknowledgments

This work was performed under financial support of the State Key Laboratory of Shale Oil and Gas Enrichment Mechanisms and Effective Development (Grant No. 33550000-22-ZC0613-0006).

References

[1] J. B. Curtis, "Fractured shale-gas systems," *AAPG Bulletin*, vol. 86, no. 11, pp. 1921–1938, 2002.

[2] D. M. Jarvie, R. J. Hill, T. E. Ruble, and R. M. Pollastro, "Unconventional shale-gas systems: the Mississippian Barnett shale of north-Central Texas as one model for thermogenic shale-gas assessment," *AAPG Bulletin*, vol. 91, no. 4, pp. 475–499, 2007.

[3] G. Liu, B. Liu, K. Liu, G. Zhai, and Z. Guo, "Silica crystallinity: characteristics and controlling factors in marine shale of the upper Yangtze area, China," *Marine and Petroleum Geology*, vol. 143, article 105833, 2022.

[4] G. Liu, G. Zhai, R. Yang, T. He, and B. Wei, "Quartz crystallinity index: new quantitative evidence for biogenic silica of the late Ordovician to early Silurian organic-rich shale in the Sichuan Basin and adjacent areas, China," *Science China Earth Sciences*, vol. 64, no. 5, pp. 773–787, 2021.

[5] S. Han, J. Zhang, Y. Li et al., "Evaluation of lower Cambrian shale in northern Guizhou Province, South China: implications for shale gas potential," *Energy & Fuels*, vol. 27, no. 6, pp. 2933–2941, 2013.

[6] T. Hu, X. Pang, F. Jiang et al., "Movable oil content evaluation of lacustrine organic-rich shales: methods and a novel quantitative evaluation model," *Earth-Science Reviews*, vol. 214, article 103545, 2021.

[7] T. Hu, X. Pang, F. Jiang et al., "Dynamic continuous hydrocarbon accumulation (DCHA): existing theories and a new unified accumulation model," *Earth-Science Reviews*, vol. 232, article 104109, 2022.

[8] G. Liu, B. Liu, Z. Huang et al., "Hydrocarbon distribution pattern and logging identification in lacustrine fine-grained sedimentary rocks of the Permian Lucaogou formation from the Santanghu basin," *Fuel*, vol. 222, pp. 207–231, 2018.

[9] R. G. Loucks, R. M. Reed, S. C. Ruppel, and D. M. Jarvie, "Morphology, genesis, and distribution of nanometer-scale pores in siliceous mudstones of the Mississippian Barnett shale," *Journal of Sedimentary Research*, vol. 79, no. 12, pp. 848–861, 2009.

[10] J. F. W. Gale, R. M. Reed, and J. Holder, "Natural fractures in the Barnett shale and their importance for hydraulic fracture treatments," *AAPG Bulletin*, vol. 91, no. 4, pp. 603–622, 2007.

[11] M. Yang, L. Li, J. Zhou, X. Qu, and D. Zhou, "Segmentation and inversion of the Hangjinqi fault zone, the northern Ordos basin (North China)," *Journal of Asian Earth Sciences*, vol. 70-71, pp. 64–78, 2013.

[12] G. Liu, Z. Huang, Z. Jiang, J. Chen, F. Chen, and J. Xing, "Gas adsorption capacity calculation limitation due to methane adsorption in low thermal maturity shale: a case study from the Yanchang Formation, Ordos Basin," *Journal of Natural Gas Science and Engineering*, vol. 30, pp. 106–118, 2016.

[13] H. Klemme and G. Ulmishek, "Effective petroleum source rocks of the world: stratigraphic distribution and controlling depositional factors," *AAPG Bulletin-American Association of Petroleum Geologists*, vol. 75, no. 12, pp. 1809–1851, 1991.

[14] W. Zhao, S. Hu, L. Hou et al., "Types and resource potential of continental shale oil in China and its boundary with tight oil," *Petroleum Exploration and Development*, vol. 47, no. 1, pp. 1–11, 2020.

[15] H. Guo, W. Jia, P. Peng et al., "The composition and its impact on the methane sorption of lacustrine shales from the Upper Triassic Yanchang Formation, Ordos Basin, China," *Marine and Petroleum Geology*, vol. 57, pp. 509–520, 2014.

[16] Q. Liu, P. Li, Z. Jin et al., "Organic-rich formation and hydrocarbon enrichment of lacustrine shale strata: a case study of Chang 7 member," *Science China Earth Sciences*, vol. 65, no. 1, pp. 118–138, 2022.

[17] W. Z. Zhang, H. Yang, S. T. Fu, and C. L. Zan, "On the development mechanism of the lacustrine high-grade hydrocarbon source rocks of Chang 91 member in Ordos Basin," *Science in China Series D-Earth Sciences*, vol. 50, no. S2, pp. 39–46, 2007.

[18] X. Wang, S. Gao, and C. Gao, "Geological features of Mesozoic lacustrine shale gas in south of Ordos Basin, NW China," *Petroleum Exploration and Development*, vol. 41, no. 3, pp. 326–337, 2014.

[19] G. Liu, Z. Huang, F. Chen et al., "Reservoir characterization of Chang 7 member shale: a case study of lacustrine shale in the Yanchang Formation, Ordos Basin, China," *Journal of Natural Gas Science and Engineering*, vol. 34, pp. 458–471, 2016.

[20] Y. Yang, W. Li, and L. Ma, "Tectonic and stratigraphic controls of hydrocarbon systems in the Ordos basin: a multicycle cratonic basin in Central China," *AAPG Bulletin*, vol. 89, no. 2, pp. 255–269, 2005.

[21] Q. L. Guo, Y. Yao, L. H. Hou, S. H. Tang, S. Q. Pan, and F. Yang, "Oil migration, retention, and differential accumulation in "sandwiched" lacustrine shale oil systems from the Chang 7 member of the Upper Triassic Yanchang Formation, Ordos Basin, China," *International Journal of Coal Geology*, vol. 261, article 104077, 2022.

[22] J. Tian, Q. Liang, F. Wang, J. Li, W. Yu, and W. Chen, "Sedimentary records of seismic events in a lacustrine basin of continental depression: a case study of the Triassic Yanchang formation in the Ordos Basin, northern China," *Journal of Asian Earth Sciences*, vol. 228, article 105128, 2022.

[23] S. Liu, "The coupling mechanism of basin and orogen in the western Ordos Basin and adjacent regions of China," *Journal of Asian Earth Sciences*, vol. 16, no. 4, pp. 369–383, 1998.

[24] W. Z. Zhang, H. Yang, S. T. Fu, and C. L. Zan, "A discussion about the development of high quality lacustrine source rocks from Chang 9-1 member in Ordos Basin," *Science in China Series D: Earth Science*, vol. 37, Supplements I, pp. 33–38, 2007.

[25] H. Yang, W. T. Dou, and X. Y. Liu, "Analysis on sedimentary faces of member 7 in Yanchang formation of Triassic in Ordos Basin," *Acta Sedimentologica Sinica*, vol. 28, no. 2, pp. 254–263, 2010.

[26] Q. H. Chen and W. H. Li, "The deep lacustrine sedimentary and its importance of oil-gas accumulation of Yanchang formation in late Triassic of Ordos Basin," *Science in China Series D: Earth Science*, vol. 37, no. 1, pp. 39–48, 2007.

[27] W. Z. Zhang, H. Yang, and Y. H. Yang, "Petroleum and element geochemistry and development environment of Yanchang formation Chang-7 high quality source rocks in Ordos Basin," *Geochemica*, vol. 37, no. 1, pp. 59–64, 2008.

[28] C. N. Zou, Z. Yang, S. Z. Tao et al., "Continuous hydrocarbon accumulation over a large area as a distinguishing characteristic of unconventional petroleum: the Ordos Basin, North-Central China," *Earth-Science Reviews*, vol. 126, pp. 358–369, 2013.

[29] H. Yang and W. Z. Zhang, "Leading effect of the seventh member high-quality source rock of Yanchang Formation in Ordos Basin during the enrichment of low-penetrating oil-gas accumulation: geology and geochemistry," *Geochimica*, vol. 34, no. 2, pp. 147–154, 2005.

[30] X. W. Qiu, C. Y. Liu, Y. H. Li, G. Z. Mao, and J. Q. Wang, "Distribution characteristics and geological significances of tuff interlayers in Yanchang Formation of Ordos Basin," *Acta Sedmentologica Sinica*, vol. 27, no. 6, pp. 1138–1146, 2009.

[31] *SY/T 5163-2010, Analysis method for clay minerals and ordinary non-clay minerals in sedimentary rocks by the X-ray diffraction*, China Petroleum Standardization Committee, 2010.

[32] J. Espitalie, J. L. Laporte, M. Madec et al., "Rapid method for source rocks characrerysation and for determination of petroleum potential and degree of evolution," *Revue De L Institut Francais Du Petrole*, vol. 32, no. 1, pp. 23–42, 1977.

[33] J. Yuqiang, D. Dazhong, Q. Lin, S. Yanfei, J. Chan, and H. Fuwei, "The basic characteristic and evaluation of shale reservoir," *Natural Gas Industry*, vol. 30, no. 10, pp. 7–12, 2010.

[34] G. Liu and D. S. Zhou, "Application of trace elements analysis in identifying sedimentary environment: taking Qianjiang Formation in the Jianghan Basin as an example," *Petroleum Geology and Experiment*, vol. 29, no. 3, pp. 307–310, 2007.

[35] E. L. Couch, "Calculation of paleo-salinities from boron and clay mineral data," *AAPG Bulletin*, vol. 55, no. 10, pp. 1829–1837, 1971.

[36] R. C. Zheng and M. Q. Liu, "Study on palaeo-salinity of Chang-6 oil reservoir set in Ordos Basin," *Oil & Gas Geology*, vol. 20, no. 1, pp. 20–25, 1999.

[37] Y. H. Fan, H. J. Qu, H. Wang, X. C. Yang, and Y. W. Feng, "The application of trace elements analysis to identifying sedimentary media environment: a case study of late Triassic strata in the middle part of western Ordos Basin," *Geology in China*, vol. 39, no. 2, pp. 382–389, 2012.

[38] J. R. Hatch and J. S. Leventhal, "Relationship between inferred redox potential of the depositional environment and geochemistry of the Upper Pennsylvanian (Missourian) Stark Shale Member of the Dennis Limestone, Wabaunsee County, Kansas, U.S.A.," *Chemical Geology*, vol. 99, no. 1-3, pp. 65–82, 1992.

[39] B. Jones and D. A. C. Manning, "Comparison of geochemical indices used for the interpretation of palaeoredox conditions in ancient mudstones," *Chemical Geology*, vol. 111, no. 1-4, pp. 111–129, 1994.

[40] M. Alberdi-Genolet and R. Tocco, "Trace metals and organic geochemistry of the Machiques Member (Aptian-Albian) and La Luna Formation (Cenomanian-Campanian), Venezuela," *Chemical Geology*, vol. 160, no. 1-2, pp. 19–38, 1999.

[41] W. H. Tonger and Y. C. X. Liu, "The discussion on anoxic environments and its geochemical identifying indices," *Acta Sedimentologica Sinica*, vol. 22, no. 2, pp. 365–372, 2004.

[42] P. H. Nadeau, D. R. Peacor, J. Yan, and S. Hillier, "I-S precipitation in pore space as the cause of geopressuring in Mesozoic mudstones, Egersund Basin, Norwegian continental shelf," *American Mineralogist*, vol. 87, no. 11-12, pp. 1580–1589, 2002.

[43] B. Thyberg and J. Jahren, "Quartz cementation in mudstones: sheet-like quartz cement from clay mineral reactions during burial," *Petroleum Geoscience*, vol. 17, no. 1, pp. 53–63, 2011.

[44] H. J. Abercrombie, I. E. Hutcheon, J. D. Bloch, and P. de Caritat, "Silica activity and the smectite-illite reaction," *Geology*, vol. 22, no. 6, pp. 539–542, 1994.

[45] B. Thyberg, J. Jahren, T. Winje, K. Bjørlykke, J. I. Faleide, and Ø. Marcussen, "Quartz cementation in Late Cretaceous mudstones, northern North Sea: changes in rock properties due to dissolution of smectite and precipitation of micro-quartz crystals," *Marine and Petroleum Geology*, vol. 27, no. 8, pp. 1752–1764, 2010.

[46] P. C. van de Kamp, "Smectite-illite-muscovite transformations, quartz dissolution, and silica release in shales," *Clays and Clay Minerals*, vol. 56, no. 1, pp. 66–81, 2008.